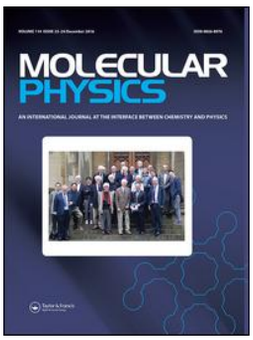

Taylor & Francis
Taylor & Francis Group

Molecular Physics

An International Journal at the Interface Between Chemistry and Physics

ISSN: 0026-8976 (Print) 1362-3028 (Online) Journal homepage: https://www.tandfonline.com/loi/tmph20

Liquid-crystal phase equilibria of Lennard-Jones chains

Bernardo Oyarzún Rivera, Thijs van Westen & Thijs J. H. Vlugt

To cite this article: Bernardo Oyarzún Rivera, Thijs van Westen & Thijs J. H. Vlugt (2016) Liquid-crystal phase equilibria of Lennard-Jones chains, Molecular Physics, 114:6, 895-908, DOI: 10.1080/00268976.2015.1134824

To link to this article: https://doi.org/10.1080/00268976.2015.1134824

Published online: 12 Jan 2016.

MOLECULAR PHYSICS, 2016
VOL. 114, NO. 6, 895–908
http://dx.doi.org/10.1080/00268976.2015.1134824

Taylor & Francis
Taylor & Francis Group

RESEARCH ARTICLE

Liquid-crystal phase equilibria of Lennard-Jones chains

Bernardo Oyarzún Rivera, Thijs van Westen and Thijs J. H. Vlugt

Process and Energy Laboratory, Delft University of Technology, Delft, The Netherlands

ABSTRACT

Liquid-crystal phase equilibria of Lennard-Jones chain fluids and the solubility of a Lennard-Jones gas in the coexisting phases are calculated from Monte Carlo simulations. Direct phase equilibria calculations are performed using an expanded formulation of the Gibbs ensemble. Monomer densities, order parameters, and equilibrium pressures are reported for the coexisting isotropic and nematic phases of: (1) linear Lennard-Jones chains, (2) a partially-flexible Lennard-Jones chain, and (3) a binary mixture of linear Lennard-Jones chains. The effect of chain length is determined by calculating the isotropic-nematic coexistence of linear Lennard-Jones chain fluids made of 8, 10, and 12 segments (8-, 10-, 12-mer). The effect of molecular flexibility on the isotropic-nematic equilibrium is studied for a Lennard-Jones 10-mer chain fluid with one freely-jointed segment at the end of the chain. An isotropic-nematic phase split and fractionation are reported for a binary mixture of linear 7-mer and 12-mer chains. Simulation results are compared with theoretical results as obtained from a recently developed analytical equation of state based on perturbation theory. Excellent agreement between theory and simulations is observed. The solubility of a monomer Lennard-Jones gas in the coexisting isotropic and nematic phases is estimated using the Widom test-particle insertion method. A linear relationship between solubility difference and density difference at isotropic-nematic coexistence is observed. It is shown that gas solubility is independent of the nematic ordering of the fluid, at constant temperature and density conditions.

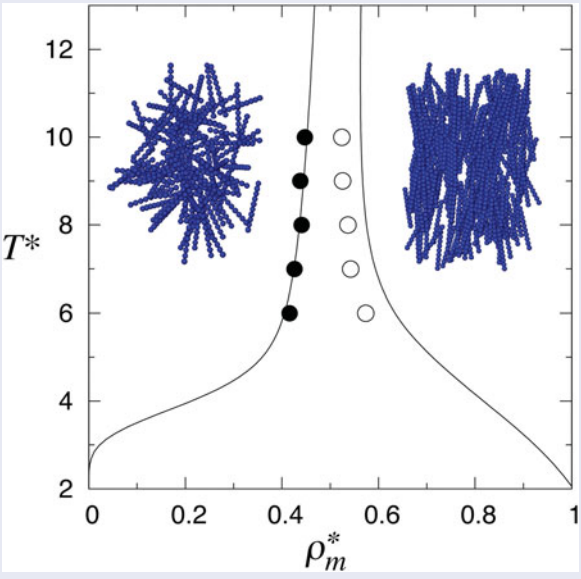

ARTICLE HISTORY
Received 7 October 2015
Accepted 14 December 2015

KEYWORDS
Molecular simulation; liquid crystals; phase equilibria

1. Introduction

Liquid crystals are elongated molecules that form fluid phases with a certain degree of molecular order. In the isotropic phase, molecules are arranged without any long-ranged orientational nor positional ordering, while in liquid-crystalline phases both orientational ordering (nematic phase) as well as positional ordering (smectic phases) are possible. In general, a certain degree of molecular anisotropy is required for the appearance of liquid-crystal phases [1,2]. Early theoretical work on the subject, i.e. the work of Onsager [3], Born [4,5], and Maier and Saupe [6–8], respectively, has shown that both repulsive and attractive interactions between molecules

CONTACT Thijs J. H. Vlugt t.j.h.vlugt@tudelft.nl

can drive the transition to a liquid-crystal phase. Nowadays, it is well understood that anisotropic repulsive molecular interactions are a necessary condition for the appearance of ordered phases [9–11], while both repulsive and attractive interactions determine the rich phase behaviour observed in liquid-crystal fluids [1,2].

Simulation and theoretical studies of complex fluids are often based on a coarse-grained description of molecules. Coarse-grained models are used to reduce the information of molecular structure into main molecular properties, summarised by a small set of model parameters. Simulations based on coarse-grained models can access longer time and length scales than their atomistic counterparts, allowing a bulk description of fluids. Coarse-grained models are commonly used to represent a simplified picture of large molecules, such as biomolecules [12–16], polymers [17–22], or liquid crystals [23–28]. Moreover, simulation results obtained from coarse-grained models can be directly compared with theoretical predictions that are based on a well-defined Hamiltonian, such as the family of perturbation theories developed from the statistical association fluid theory (SAFT) [29–36]. While, traditionally, this relation between fluid theories and molecular simulations was primarily used for the development of improved theories, more recent developments show that this is not a one-way street, as accurate SAFT-type theories also provide a very efficient means to derive coarse-grained force fields for use in molecular simulations [20,22,37–42] (see Ref. [21] for a recent review).

Typically, coarse-grained models use simple expressions for the interaction energies. Pair-interaction potentials as hard-sphere [43–49], hard-ellipsoid [50–52], hard-spherocylinders [53–55], and the Gay-Berne potential [56–61] are popular for studying liquid crystals. Other more elaborated interaction models have been proposed, e.g. hard-spherocylinder with an attractive square-well potential [28,62–64], hard-disc with an anisotropic square-well attractive potential [27], hard-spherocylinder with an attractive Lennard-Jones potential [65], anisotropic soft-core spherocylinder potential [66,67], and copolymers [68–70]. In this work, we focus our study on the isotropic-nematic phase behaviour of linear and partially-flexible Lennard-Jones chain fluids. To the best of our knowledge, apart from our recent work [71], there is no other study showing simulation results for the isotropic-nematic phase transition of Lennard-Jones chains. Galindo *et al.* [72] studied the phase behaviour of linear Lennard-Jones chains of 3 and 5 segments; however, in that study, no liquid-crystalline phases were observed due to the short length of the chains. The importance of this study is twofold, first to determine the effect of main molecular characteristics (such as chain length, flexibility, attractive interactions, and composition of mixtures) on the isotropic-nematic behaviour of long Lennard-Jones chains, and second to validate the analytical equation of state presented by van Westen *et al.* [71] for Lennard-Jones chain fluids with variable degree of flexibility.

The equation of state of van Westen *et al.* [71] was developed using a perturbation theory based on a reference fluid of hard-chain molecules. An important assumption in the development of the equation of state was that of orientation-independent attractive interactions. As shown in Ref. [71], this assumption leads to an excellent description of the isotropic-nematic phase behaviour of a linear Lennard-Jones 10-mer fluid. We here provide a more elaborate evaluation of the equation of state comparing it to simulation data, allowing further analysis on the effect of molecular orientation on attractive dispersion interactions.

An important property of liquid crystals, relevant for technological applications, is the solubility of gases in them. Recently, liquid crystals have been proposed as new solvents for CO_2 capture [73–77]. The principle behind this application is the drop in the solubility of gases observed at the fluid–fluid transition from the isotropic to the nematic phase [74,78,79]. This phase change is associated with a very low enthalpy of transition $\Delta H^{\text{N-I}} \sim$ 1–10 kJ/mol, taking place at a broad range of temperature and pressure conditions [80]. In this work, we use molecular simulations to analyse the effect of density, temperature, and composition of mixtures, on the solubility difference of gases between the coexisting isotropic and nematic phases.

This paper is organised as follows. In Section 2, we describe briefly the expanded Gibbs ensemble simulation method for the direct calculation of the phase equilibrium between two phases. In Section 3, results are presented for the isotropic-nematic phase equilibria of linear Lennard-Jones chain fluids (Section 3.1), partially-flexible Lennard-Jones chain fluids (Section 3.2), and a binary mixture of linear Lennard-Jones chains (Section 3.3). Solubility results for a Lennard-Jones gas in the coexisting isotropic and nematic phases of the studied systems are presented in Section 3.4. Our results are summarised in Section 4.

2. Molecular model and simulation methods

In this work, we study the isotropic-nematic phase equilibria of linear and partially-flexible Lennard-Jones chains. A chain molecule is defined as a molecule made of spherical segments connected by a rigid segment-to-segment bond length equal to the segment diameter σ. A linear chain is defined as a chain molecule with all

segments on the same axis. Linear chains with m segments are identified as a linear m-mer. Partially-flexible chain molecules are made of a linear part and a freely-jointed flexible part. The partially-flexible model is proposed in similarity with real liquid-crystal molecules, formed by a rigid core and a flexible tail. The freely-jointed part is not governed by any bond-bending or torsional potential, therefore, it is free to adopt any possible molecular configuration subject to the constraints of a rigid bond length and the pair potential interaction between segments. A partially-flexible chain molecule of m segments in total and m_R segments in the rigid block is denoted as a partially-flexible m-m_R-mer [81].

The pair potential between two segments i and j separated by a distance r_{ij} is defined by the Lennard-Jones potential,

$$u_{ij}(r) = 4\epsilon \left[\left(\frac{\sigma}{r_{ij}} \right)^{12} - \left(\frac{\sigma}{r_{ij}} \right)^{6} \right], \qquad (1)$$

where ϵ is the depth of the potential well and σ is the segment diameter identified as the zero-potential distance between two segments. ϵ and σ are constant for all segment pair-interactions considered in this work. Intermolecular pair interactions are evaluated for segments of different molecules and for segments of the same molecule that are separated by two or more bonds. All magnitudes reported in this study are dimensionless with ϵ as the basis for energy and σ as the basis for length. Some of these magnitudes are: reduced temperature $T^* = k_B T/\epsilon$, where T is the temperature and k_B is the Boltzmann constant; reduced monomer density $\rho_m^* = mN\sigma^3/V$, where N is the number of molecules; and reduced pressure $P^* = P\sigma^3/k_B T$, where P is the pressure of the system. In a binary mixture, the reduced monomer density is defined as $\rho_m^* = (m_1 x_1 + m_2 x_2)N\sigma^3/V$, where x_1 and x_2 are the mole fraction of the short and long chain, respectively.

Phase equilibria calculations are performed in an expanded version of the Gibbs ensemble [49,82,83]. A brief explanation of the method is given here, while a detailed description can be found in our previous work [49]. Two forms of the method are distinguished: a constant volume ensemble in which the total volume of the system (the volume of both simulation boxes) remains unchanged, and a constant pressure ensemble in which the pressure of the system is defined and the volume of each simulation box is varied independently. In both cases, the partition function is defined for a constant total number of molecules and temperature. Constant volume simulations are used for the calculation of single component systems, while constant pressure simulations are used in the case of mixtures. In an expanded formulation of the Gibbs ensemble, molecular transfer is performed by a gradual exchange of molecules between phases. Different methods have been proposed for this gradual transfer: configurational-bias insertions/deletions of segments of a tagged molecule [82,84,85], continuous coupling of the intermolecular interactions of a fractional molecule [83,86,87], and discrete coupling of the segments of a fractional molecule [49]. Here, we use the discrete-coupling method for the gradual transfer of a fractional chain molecule. A fractional chain molecule is defined as a molecule that has a varying number of interacting segments (pair interactions). The number of interacting segments is determined by the coupling state λ, ranging from $\lambda = 0$ for a fractional molecule that experiences only bonded interactions, to $\lambda = m_i$ (the total number of segments of a chain molecule of type i) for a fractional molecule that fully interacts with itself and the other molecules. We distinguish between fractional molecules, where changes in the coupling state takes place, and whole molecules, which are not subject to changes in their coupling state. There is one fractional molecule in each phase per component type i. It is important to note that a fractional molecule in the coupling state m_i is identical to a whole molecule, but it is only considered as a whole molecule after molecular transfer takes place. Molecular transfer is defined as the state change in the coupling parameter from m_i of an old fractional molecule to 0 of a new fractional molecule. When molecular transfer takes place, the fractional molecule becomes a new whole molecule and a new fractional molecule without any pair interactions (but with bonded interactions) is randomly inserted in the system. In the case of partially-flexible molecules, a new molecule with random molecular configuration is inserted. In the phase where the molecule is transferred from, a new fractional molecule is chosen randomly from all other whole molecules of the same species. Fractional molecules are subjected to all Monte Carlo trial moves irrespectively of their coupling state.

In the standard Boltzmann sampling, intermediate coupling states are rarely visited, limiting the efficiency of the method. Therefore, weight functions for each coupling state are introduced to bias the Boltzmann statistics of the system. The weight functions are not known *a priori* and an iterative method is required for their calculation. The Wang–Landau sampling method is used for shifting the density of states in the coupling parameter space towards uniform sampling [88,89]. Equilibrium properties of the unweighted system are recovered by accumulating weighted averages over the Markovian process.

The pair potential of Equation (1) is truncated at a cut-off radius $r_c = 2.5\sigma$ and the usual long-range tail corrections are applied [90,91]. The contribution of the fractional molecules to the tail corrections is neglected, as this energy contribution is very small. The pressure of the system is calculated by the molecular virial for chain molecules in a system with periodic boundaries as described by Theodorou *et al.* [92].

At every Monte Carlo step, one of the following trial moves is attempted: displacement, rotation, reptation, configurational-bias partial regrowth (only for partially flexible molecules) [91], volume change, identity exchanges [93] (only for mixtures of linear chains), and coupling parameter change. Trial moves are selected randomly with a fixed probability proportional to the ratio 100:100:10:100:1:100:1000, respectively. Volume changes are performed isotropically in the logarithm of the volume. Initial isotropic configurations are placed in a cubic box, while initial nematic configurations are placed in a rectangular box with an edge length ratio of 1:1.1:1.2. Periodic boundary conditions are used in all systems. The maximum displacement, rotation, volume, and coupling parameter changes are adjusted for a maximum acceptance ratio of 20%. A Monte Carlo cycle consists of a number of trial moves equal to the total number of molecules in the system ($\sim 1 \times 10^3$). Equilibration requires typically 3×10^6 cycles and averages were collected in 2×10^6 production cycles.

Nematic phases are characterised by the order parameter S_2, defined as the average of the second-order Legendre polynomial $P_2(\cos\theta)$ [1,2],

$$S_2 = \left\langle \frac{1}{N}\sum_{i=1}^{N} P_2(\cos\theta_i) \right\rangle = \frac{3}{2}\left\langle \frac{1}{N}\sum_{i=1}^{N}\left(\cos^2\theta_i - \frac{1}{3}\right)\right\rangle, \tag{2}$$

where θ_i is the angle between the molecular axis of molecule i and the nematic director. This definition of the order parameter requires two iterations over the total number of molecules, a first for determining the nematic director and second for calculating the order parameter itself. Alternatively, the order parameter can be calculated from the largest eigenvalue of the *de Gennes* **Q**-tensor [1], which represents the maximum difference of the second-order tensor between the ordered phase and a perfect isotropic phase [48,94]: $\mathbf{Q} = \frac{1}{N}\sum_{i=1}^{N}(\mathbf{q}_i\mathbf{q}_i - \frac{1}{3}\mathbf{I})$, where $\mathbf{q}$ is a unit vector that identifies the direction of the molecular axis with respect to the laboratory frame. The order parameter S_2 is proportional to the ensemble average of the largest eigenvalue of the **Q**-tensor, $S_2 = \frac{3}{2}\langle\lambda_+\rangle$. A value of S_2 close to 0 indicates the presence of an isotropic phase and a value close to 1 indicates nematic ordering. The molecular axis of partially-flexible molecules is defined as the eigenvector corresponding to the smallest eigenvalue of the moment of inertia tensor [46].

Positional ordering is detected by the smectic order parameter, which is defined by the magnitude of the first Fourier component of the normalised density wave along the nematic director [95,96],

$$\tau = \frac{1}{N}\left|\sum_{j=1}^{N} e^{ik_z z_j}\right|. \tag{3}$$

In this equation, $k_z = 2\pi/\lambda_z$, where λ_z is the periodicity of the smectic layers, and z_j is the coordinate of the centre of mass of the jth molecule in the direction of the nematic director. Values of the smectic order parameter, which differ significantly from zero, indicate the presence of smectic layers.

Infinite dilution solubility of gases is expressed as a dimensionless Henry coefficient defined by $H_k^*(T,\rho,\mathbf{x}) = H_k(T,\rho,\mathbf{x})/\rho k_B T$, where H_k is the Henry coefficient of component k in a fluid with number density of molecules ρ and mole fraction $\mathbf{x}$. Dimensionless Henry coefficients are related to the infinite dilution residual chemical potential $\mu_k^{res}(T,\rho,\mathbf{x})$ of a gas in a solvent [97], and are calculated in constant pressure Monte Carlo simulations using the Widom test-particle insertion method [98,99],

$$\ln H_k^*(T,\rho',\mathbf{x}) = \frac{\mu_k^{res}(T,\rho',\mathbf{x})}{k_B T} = -\ln\frac{\langle V\exp[-\beta U^{ins}]\rangle}{\langle V\rangle}. \tag{4}$$

It has to be noticed that, in this equation $\rho' = \langle N/V\rangle$ is the average density of the fluid at constant temperature and pressure conditions. The insertion energy U^{ins} is equal to the energy change when a Lennard-Jones segment is temporary placed at a random position in the fluid. The infinite dilution solubility of a Lennard-Jones segment is measured in both the coexisting isotropic and nematic phase at equilibrium. Equilibrium configurations are sampled every 1×10^3 Monte Carlo cycles in which a total of 100 test-particle insertions are attempted.

3. Results

The simulation results presented in this section are extensively compared to a recently developed analytical equation of state of van Westen *et al.* [71]. The equation of state was developed from a perturbation theory based on a hard-chain reference fluid. The Helmholtz energy as obtained from the equation of state can, thus, be written

Table 1. Isotropic (I) and nematic (N) phase equilibria of linear Lennard-Jones m-mer chain fluids as a function of reduced temperatures T^*. For each phase, reduced monomer densities ρ_m^*, order parameters S_2, and reduced pressures P^*, are reported. Reported statistical uncertainties are equivalent to one standard deviation.

T^*	$\rho_m^{*,\mathrm{I}}$	S_2^{I}	$P^{*,\mathrm{I}}$	$\rho_m^{*,\mathrm{N}}$	S_2^{N}	$P^{*,\mathrm{N}}$
			$m = 8$			
10	0.569 ± 0.005	0.132 ± 0.059	4.809 ± 0.062	0.614 ± 0.004	0.685 ± 0.051	4.810 ± 0.065
9	0.561 ± 0.004	0.168 ± 0.053	4.026 ± 0.058	0.607 ± 0.003	0.689 ± 0.051	4.030 ± 0.059
8	0.554 ± 0.004	0.196 ± 0.060	3.269 ± 0.031	0.602 ± 0.003	0.709 ± 0.018	3.269 ± 0.030
7	0.542 ± 0.004	0.141 ± 0.041	2.562 ± 0.025	0.604 ± 0.003	0.747 ± 0.023	2.561 ± 0.026
6	0.541 ± 0.005	0.262 ± 0.078	1.881 ± 0.033	0.600 ± 0.004	0.744 ± 0.030	1.881 ± 0.033
5	0.528 ± 0.007	0.243 ± 0.082	1.202 ± 0.018	0.614 ± 0.005	0.813 ± 0.021	1.201 ± 0.018
			$m = 10$			
10	0.446 ± 0.002	0.144 ± 0.042	2.275 ± 0.114	0.523 ± 0.002	0.789 ± 0.009	2.275 ± 0.112
9	0.438 ± 0.002	0.138 ± 0.046	1.919 ± 0.017	0.526 ± 0.003	0.801 ± 0.011	1.919 ± 0.015
8	0.441 ± 0.006	0.198 ± 0.081	1.567 ± 0.025	0.537 ± 0.004	0.828 ± 0.009	1.566 ± 0.024
7	0.427 ± 0.004	0.192 ± 0.070	1.168 ± 0.016	0.542 ± 0.004	0.849 ± 0.005	1.165 ± 0.015
6	0.416 ± 0.007	0.225 ± 0.052	0.805 ± 0.012	0.573 ± 0.006	0.893 ± 0.008	0.803 ± 0.013
			$m = 12$			
12	0.376 ± 0.004	0.081 ± 0.021	1.825 ± 0.044	0.463 ± 0.011	0.820 ± 0.023	1.823 ± 0.045
11	0.371 ± 0.004	0.085 ± 0.017	1.577 ± 0.036	0.467 ± 0.010	0.834 ± 0.015	1.576 ± 0.036
10	0.366 ± 0.002	0.087 ± 0.015	1.337 ± 0.012	0.472 ± 0.006	0.846 ± 0.014	1.335 ± 0.013
9	0.357 ± 0.004	0.085 ± 0.023	1.078 ± 0.023	0.479 ± 0.007	0.862 ± 0.008	1.077 ± 0.023
8	0.347 ± 0.005	0.085 ± 0.018	0.833 ± 0.026	0.493 ± 0.011	0.882 ± 0.011	0.831 ± 0.026
7	0.326 ± 0.004	0.072 ± 0.007	0.579 ± 0.014	0.520 ± 0.011	0.909 ± 0.010	0.576 ± 0.015

as a sum of different contributions, according to

$$\frac{A}{Nk_{\mathrm{B}}T} = \frac{A^{\mathrm{id}}}{Nk_{\mathrm{B}}T} + \frac{A^{\mathrm{hc}}}{Nk_{\mathrm{B}}T} + \frac{A^{\mathrm{disp}}}{Nk_{\mathrm{B}}T}. \tag{5}$$

Here, A^{id} is an ideal gas contribution, A^{hc} is a Helmholtz energy due to chain formation, and A^{disp} is a contribution due to attractive dispersion interactions. The hard-chain term was obtained from a rescaled Onsager theory, based on the Onsager trial function for describing the orientational distribution function of the molecules. The dispersion term was developed using a second-order Barker-Henderson theory [100,101], based on the radial distribution function of hard-chain molecules in the isotropic phase. The dispersion contribution is, therefore, independent on the orientation of the molecules. For details on the equations for calculating the different contributions, the reader is referred to the work of van Westen *et al.* [71]. Details on the development of the different contributions to the equation of state can be found elsewhere [81,102–105].

Previously, the equation of state was applied to pure fluids only. Here, it is also applied to mixtures. The extension of the equation of state to mixtures is straightforward, and can be obtained from Ref. [104] (chain contribution) and Ref. [105] (dispersion contribution).

3.1. Linear Lennard-Jones chains

The liquid-crystal phase equilibria of linear Lennard-Jones 8-, 10- and 12-mers were calculated from constant volume expanded Gibbs ensemble simulations. Initial estimates of densities in the coexisting isotropic and nematic phases were obtained from the equation of state of van Westen *et al.* [71]. Results for the linear 10-mer fluid were already shown in our previous work [71], and results reported here were obtained from longer simulation runs. Reduced monomer densities, order parameters, and reduced pressures at the isotropic-nematic coexistence are shown in Table 1 as a function of reduced temperature. Temperature–density phase diagrams are shown in Figure 1 together with theoretical results obtained from the equation of state. It can be observed that for longer chains, the isotropic-nematic equilibrium is shifted towards lower densities while the density difference between both coexisting phases is increased. Lower equilibrium densities and larger density differences are a consequence of larger excluded volume differences between the isotropic and the nematic phase as the chain length increases [106]. For longer chains, the pair-excluded volume is more anisotropic than for shorter chains, resulting in a larger driving force for the isotropic-nematic transition. Values for the order parameter in the isotropic phase deviate systematically from 0 due to the finite size of the system. Eppenga *et al.* [94] derived a relation between the size of the system and

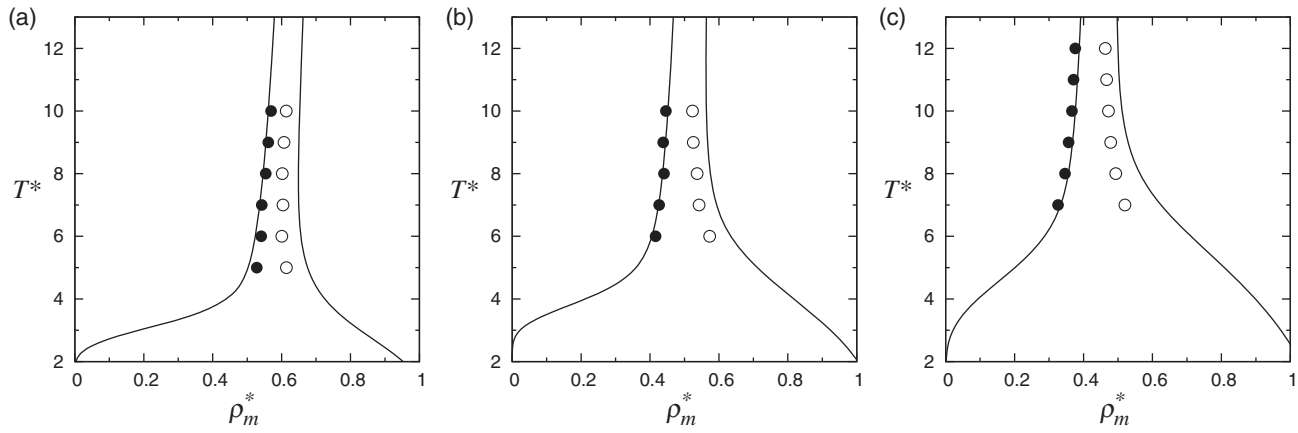

Figure 1. Isotropic-nematic phase equilibria of linear Lennard-Jones chain fluids: (a) 8-mer, (b) 10-mer, and (c) 12-mer. Reduced temperature T^* vs. reduced monomer density ρ_m^*. Filled (•) and open (○) symbols are simulation results for the isotropic and nematic phase, respectively. Solid lines are theoretical results obtained from the analytical equation of state of van Westen *et al.* [71].

values of the order parameter in the isotropic phase, showing that the offset from zero is equal to $1/\sqrt{N}$. In our previous work [48], we showed the validity of this relation for a system of hard-sphere chain molecules. In the systems studied here, the average number of molecules in the isotropic phases was typically: 500 for the 12-mer system, 200 for the 10-mer, and 300 for the 8-mer.

As it is shown in Figure 1, the theoretical results as obtained from the perturbation theory of van Westen *et al.* provide an overall excellent description of the isotropic-nematic phase diagram. Nevertheless, some minor deviations can be observed. The small but systematic overestimation of nematic equilibrium densities is expected, since densities in the nematic phase are already overestimated in the description of the hard-chain reference fluid [103]. These small overestimations are a result of the approximations made for describing higher (third, fourth, etc.) virial coefficients in the rescaled Onsager approach for hard-chain fluids. Equilibrium densities of the isotropic phase are slightly different from simulation results, with an increasing deviation for longer chain lengths. Albeit the deviations are small, the increasing deviation with chain length cannot be explained from the behaviour of the reference fluid [103], since the description of the hard-chain reference system improves for longer chain lengths. Figure 2 shows the reduced pressure vs. reduced temperature diagram at isotropic-nematic coexistence for linear Lennard-Jones chain fluids. In this figure, it can be clearly identified that the theoretical description of the isotropic-nematic phase equilibria is less accurate as the chain length increases. Figures 1 and 2 suggest that the theoretical description misses a small (positive) contribution to the driving force for the isotropic to nematic phase transition. van Westen *et al.* assumed that

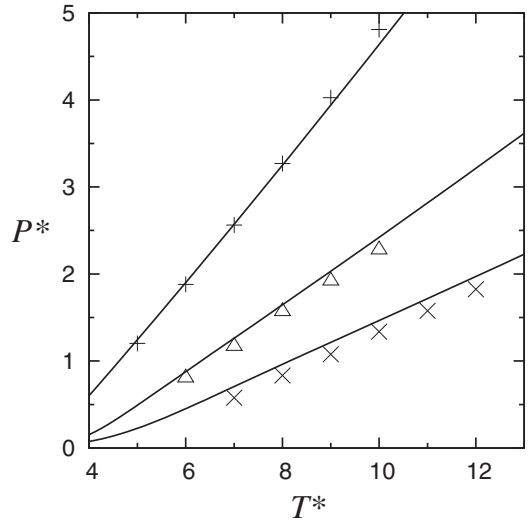

Figure 2. Reduced temperature T^* vs. reduced pressure P^* at the isotropic-nematic coexistence for linear Lennard-Jones 8-mer (+), 10-mer (△), and 12-mer (×) chain fluids. Solid lines are theoretical results obtained from the analytical equation of state of van Westen *et al.* [71].

no explicit orientation dependent contribution in the dispersive Helmholtz energy was required for a reliable description of the isotropic-nematic phase equilibria of Lennard-Jones chain fluids [71]. The results shown here indicate that this assumption may be less justified for longer chains, wherefore, a stronger effect of anisotropic interactions is expected. Another theoretical assumption that could explain the observed deviations is the use of a fixed temperature-independent aspect ratio of the molecules. This assumption is typically needed in a perturbed-chain approach [105]; however, it reduces the driving force for the isotropic to nematic phase transition as the aspect ratio should slightly increase with temperature (see e.g. Ref. [67]). An increased aspect

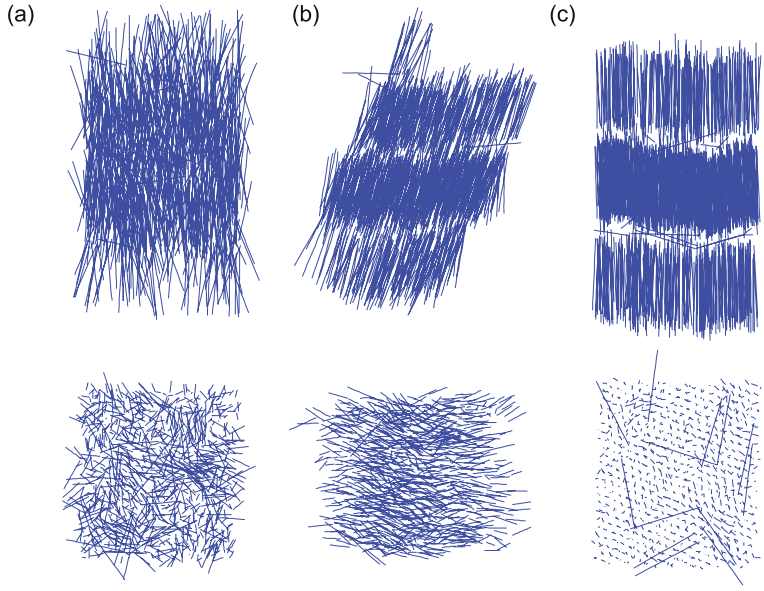

Figure 3. Typical snapshots of ordered phases for a linear Lennard-Jones 10-mer chain fluid at coexistence between an isotropic phase and: (a) a nematic phase at $T^* = 6$, (b) a smectic-C phase at $T^* = 5$, and (c) a crystal phase at $T^* = 4$. The top row shows parallel views and the bottom row shows perpendicular views to the largest axis of the simulation box.

ratio would lead to a more anisotropic molecule and, therefore, a higher driving force for the phase transition. In summary, we find systematic but small deviations between theory and simulations that could be caused by the assumption of orientation-independent attractions or a fixed aspect ratio of the molecules. We conclude that this assumption do not diminish an accurate description of the phase equilibrium.

Figure 2 shows a linear relationship between pressure and temperature at the isotropic-nematic coexistence for linear Lennard-Jones chain fluids. Further analysis is obtained considering the Clapeyron equation, $dP/dT = \Delta h^{\text{I-N}}/(T\Delta v^{\text{I-N}})$, where $\Delta h^{\text{I-N}}$ is the enthalpy change at the isotropic-nematic phase transition, and $\Delta v^{\text{I-N}}$ is the molar volume change between both phases at coexistence. A constant slope dP^*/dT^* indicates a proportional relationship between enthalpy change and volume change. It is remarkable that energetic and density effects at the isotropic-nematic phase transition are directly coupled, suggesting that any energetic change at the phase transition can be described from the isotropic-nematic density change and vice versa.

At temperatures lower than the ones reported in Figure 1 and Table 1, isotropic-smectic and isotropic-solid phase coexistence is found. Figure 3 shows typical snapshots for a sequence of nematic, smectic-C, and crystal phases for a linear 10-mer fluid as temperature decreases. A similar picture of crystal and smectic-C phases of a 10-mer fluid at a constant monomer density of $\rho_m^* = 0.8$ was reported by Affouard *et al.* [107]. In the smectic-C phase, molecules are positioned in layers and oriented with the nematic director tilted with respect to the normal of the layers. Smectic phases were detected by the smectic order parameter (Equation (3)) and identified as smectic-C phases by inspecting snapshots of final configurations. Table 2 shows the results for the observed coexistence between isotropic and smectic-C phases. These data should be considered only as preliminary due to small differences (∼5%) in the calculated pressure of both coexisting phases. This difference is a consequence of the difficulties in arranging the tilted oriented layers in the periodically repeating rectangular box. In the crystal phases, molecules are arranged in layers with the molecular axis pointing in the direction of the normal of

Table 2. Isotropic (I) and smectic-C (SmC) phase equilibria of linear Lennard-Jones *m*-mer chain fluids.

m	T^*	$\rho_m^{*,\text{I}}$	S_2^{I}	$P^{*,\text{I}}$	$\rho_m^{*,\text{SmC}}$	S_2^{SmC}	$P^{*,\text{SmC}}$
8	4	0.468 ± 0.021	0.178 ± 0.101	0.471 ± 0.026	0.699 ± 0.031	0.924 ± 0.021	0.447 ± 0.032
10	5	0.335 ± 0.007	0.101 ± 0.009	0.338 ± 0.015	0.688 ± 0.010	0.965 ± 0.005	0.309 ± 0.015
12	6	0.308 ± 0.015	0.087 ± 0.016	0.372 ± 0.030	0.673 ± 0.032	0.977 ± 0.007	0.348 ± 0.024

Table 3. Isotropic (I) and nematic (N) phase equilibria of the partially-flexible Lennard-Jones 10-9-mer chain fluid.

T^*	$\rho_m^{*,\mathrm{I}}$	S_2^{I}	$P^{*,\mathrm{I}}$	$\rho_m^{*,\mathrm{N}}$	S_2^{N}	$P^{*,\mathrm{N}}$
10	0.568 ± 0.007	0.227 ± 0.120	4.558 ± 0.048	0.597 ± 0.002	0.601 ± 0.035	4.562 ± 0.045
9	0.564 ± 0.006	0.283 ± 0.123	3.823 ± 0.033	0.599 ± 0.002	0.685 ± 0.021	3.824 ± 0.036
8	0.559 ± 0.004	0.171 ± 0.061	3.187 ± 0.029	0.600 ± 0.002	0.710 ± 0.019	3.189 ± 0.023
7	0.560 ± 0.005	0.265 ± 0.102	2.518 ± 0.021	0.600 ± 0.002	0.726 ± 0.020	2.519 ± 0.022
6	0.555 ± 0.010	0.295 ± 0.060	1.831 ± 0.013	0.601 ± 0.002	0.745 ± 0.007	1.828 ± 0.016
5	0.543 ± 0.006	0.294 ± 0.108	1.101 ± 0.032	0.605 ± 0.002	0.781 ± 0.013	1.105 ± 0.028

the layers. Vega *et al.* [108] described the possible crystal phases of hard-sphere dumbbells from closest packing considerations. These authors identified that dumbbells should be arranged in layers with their axis parallel but tilted from the normal layer by approximately 35°. In that study, the stacking of layers was considered in three different ways, forming an ABAB (hexagonal close packed), or an ABC (face-centred cubic) sequence, or a sequence where layers are stacked alternating the tilted angles between successive layers. Galindo *et al.* [72] considered the ABC sequence in the solid phases of linear Lennard-Jones chains, while Polson *et al.* [109] suggested that an AAA (body-centred cubic) stacking with a tilt angle of approximately 33° is the stable configuration for the crystal phase of a 6-mer Lennard-Jones fluid with finite bending potential. Simulations showing crystal phases are considered only as an indication of the formation of solid phases. This is because of large pressure differences observed between both coexisting phases and the known difficulties in performing direct phase equilibrium calculations of systems including solids [91,109–111].

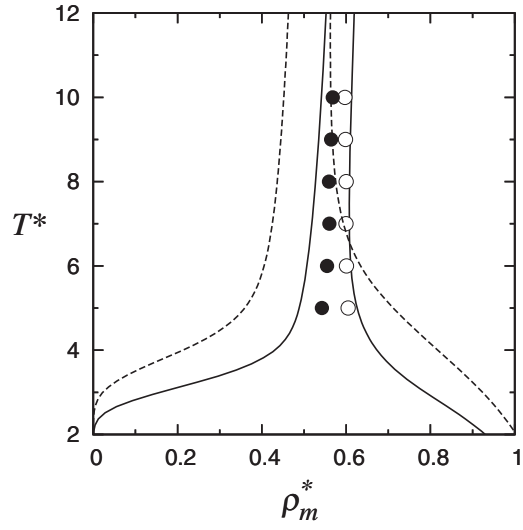

Figure 4. Isotropic-nematic phase equilibria of the partially-flexible Lennard-Jones 10-9-mer compared to the linear Lennard-Jones 10-mer chain fluid. Reduced temperature T^* vs. reduced monomer density ρ_m^*. Symbols and solid lines for the partially-flexible 10-9-mer fluid as in Figure 1. Dashed lines are theoretical results for the linear 10-mer fluid.

3.2. Partially-flexible Lennard-Jones chains

The effect of molecular flexibility on the isotropic-nematic phase equilibria of Lennard-Jones chain fluids is studied for a partially-flexible 10-9-mer fluid. Table 3 reports the simulation data and Figure 4 compares the isotropic-nematic coexistence densities of the partially-flexible 10-9-mer to those of the linear 10-mer fluid. It can be observed that the effect of flexibility is twofold: (1) it increments the densities at which the phase transition takes place, and (2) it reduces the density difference between both phases. These observations can be explained from the fact that the pair-excluded volume of partially-flexible chains is less anisotropic than that of linear chains [81], thereby constituting a smaller driving force for the isotropic to nematic phase transition. The average number of molecules in the isotropic phases was around 200 for all the temperature conditions considered here.

Another effect of flexibility is the appearance of smectic phases at a temperature lower than the one observed for the linear chain fluid. At $T^* = 5$, isotropic-nematic equilibrium is observed for the 10-9-mer fluid while isotropic-smectic coexistence was found for the linear 10-mer fluid at the same temperature. Our observations suggest that the temperature of the isotropic-nematic-smectic triple point of Lennard-Jones chain fluids decreases with increasing flexibility, i.e. decreasing molecular anisotropy. A similar behaviour was observed in the case of Gay-Berne fluids with different shape anisotropy [112–114]. At reduced temperatures, lower than the ones reported in Figure 4 and Table 3, smectic and crystal phases were observed, similarly as described in the previous section.

3.3. Binary mixture of linear Lennard-Jones chains

Constant pressure expanded Gibbs-ensemble simulations are performed for determining the isotropic-nematic

Table 4. Isotropic (I) and nematic (N) phase equilibria of the binary mixture of linear Lennard-Jones 7-mer and 12-mer chains at $P^* = 2.535$. x_2 is the mole fraction of the long chain (12-mer).

T^*	x_2^{I}	$\rho_m^{*,\mathrm{I}}$	S_2^{I}	x_2^{N}	$\rho_m^{*,\mathrm{N}}$	S_2^{N}
14	0.971 ± 0.001	0.402 ± 0.012	0.143 ± 0.081	0.988 ± 0.001	0.489 ± 0.000	0.844 ± 0.002
13	0.766 ± 0.011	0.407 ± 0.003	0.157 ± 0.052	0.904 ± 0.007	0.505 ± 0.001	0.837 ± 0.010
12	0.606 ± 0.011	0.418 ± 0.002	0.098 ± 0.009	0.845 ± 0.008	0.530 ± 0.001	0.857 ± 0.006
11	0.463 ± 0.018	0.431 ± 0.003	0.092 ± 0.020	0.787 ± 0.013	0.556 ± 0.002	0.874 ± 0.008
10	0.340 ± 0.010	0.448 ± 0.002	0.069 ± 0.010	0.770 ± 0.015	0.605 ± 0.002	0.908 ± 0.009
9	0.222 ± 0.017	0.467 ± 0.003	0.065 ± 0.006	0.716 ± 0.040	0.637 ± 0.004	0.920 ± 0.014
8	0.124 ± 0.010	0.491 ± 0.002	0.062 ± 0.008	0.668 ± 0.041	0.680 ± 0.002	0.938 ± 0.011
7	0.050 ± 0.001	0.522 ± 0.001	0.063 ± 0.008	0.521 ± 0.009	0.706 ± 0.001	0.938 ± 0.004
6	0.014 ± 0.004	0.566 ± 0.001	0.092 ± 0.023	0.402 ± 0.041	0.788 ± 0.048	0.959 ± 0.013
5.397	0.000 ± 0.000	0.606 ± 0.004	0.156 ± 0.040	0.000 ± 0.000	0.631 ± 0.004	0.517 ± 0.081

phase equilibria of a binary mixture of linear Lennard-Jones 7-mer and 12-mer chains (7-mer+12-mer). Table 4 reports numerical results and Figure 5 shows a comparison between simulation results and theoretical predictions obtained from the analytical equation of state of van Westen *et al.* [71]. As before, an offset of 0 is observed in the values for the order parameter for the isotropic phase. The average number of molecules in the isotropic phase ranges from approximately 70 at the highest temperature to around 600 at $T^* = 9$.

Phase split between an isotropic and a nematic phase and fractionation of the fluid between both phases is observed. Fractionation of the mixture into an isotropic phase richer in the short chains and a nematic phase richer in the long chains is a consequence of the more anisotropic pair-excluded volume interactions of the long chains. Figure 5(a) shows the mole fraction of the long chain x_2 in the isotropic and nematic phases at different equilibrium temperatures. An accurate description of fractionation between both phases is obtained from theoretical calculations. Figure 5(b) compares simulation results for the isotropic and nematic coexistence monomer densities with theoretical results from the equation of state. At constant mole fraction, a maximum in the density of the nematic phase and a maximum in the isotropic-nematic density difference is observed in the range $x_2 = 0.4 - 0.6$ from simulation results and at $x_2 = 0.5$ from the theoretical results. Previously, a similar behaviour was found for binary mixtures of linear hard-sphere chains [49,104]. With increasing mole fraction of the long component, the driving force for the phase transition increases, which leads to lower coexistence densities. However, the addition of a small amount of the long component to a pure fluid of the short component leads to a dramatic increase in the orientational order of the system (due to induced order [104]). As a result, the density of the nematic phase increases. These two competing effects lead to the observed maximum. Overall, comparison between theory and simulations is accurate. A slight overestimation of the isotropic and nematic monomer

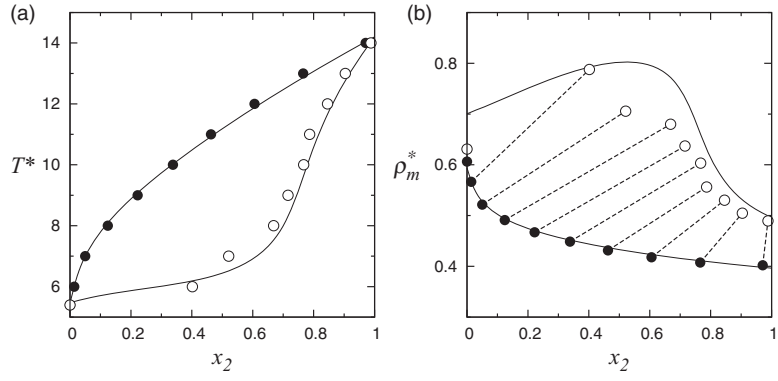

Figure 5. Isotropic-nematic phase equilibria for a binary mixture of linear Lennard-Jones 7-mer and 12-mer chains at a reduced pressure of $P^* = 2.535$. (a) Reduced temperature T^* and (b) reduced monomer density ρ_m^* vs. mole fraction of the largest component x_2. Symbols and solid lines as in Figure 1. Dashed lines are constant temperature tie-lines as reported in Table 4. Pure component simulation data for the 7-mer fluid are calculated from constant volume expanded Gibbs-ensemble simulations at temperatures close to the equilibrium temperature. Equilibrium temperature and isotropic-nematic coexisting densities at the specified pressure of the mixture are determined by interpolation from the closest calculated equilibrium pressures.

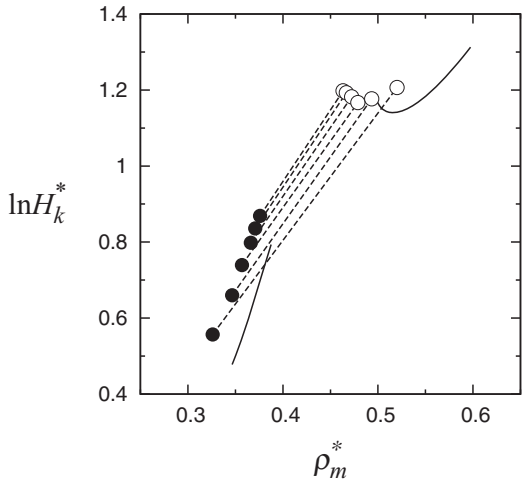

Figure 6. Infinite dilution solubility of a Lennard-Jones gas in the coexisting isotropic and nematic phases of a linear Lennard-Jones 12-mer chain fluid. Symbols and solid lines as in Figure 1. Dashed lines are constant temperature tie-lines as reported in Table 1.

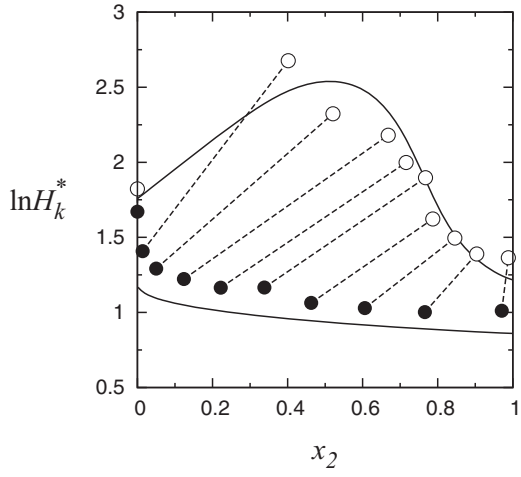

Figure 7. Infinite dilution solubility of a Lennard-Jones gas in the coexisting isotropic and nematic phases of a binary mixture of linear Lennard-Jones 7-mer and 12-mer chains. Logarithm of dimensionless Henry coefficient ln H_k^* vs. mole fraction of the long chain x_2. Symbols and solid lines as in Figure 1. Dashed lines are constant temperature tie-lines as reported in Table 4.

densities is observed, with larger deviations at lower temperatures corresponding to a larger concentration of the short chains. This effect is expected since the description of the hard-chain reference fluid that underlies the perturbation theory becomes less accurate for shorter chain lengths [104].

3.4. Solubility of gases in Lennard-Jones chains

In this section, we study the infinite dilution solubility of a Lennard-Jones gas in the coexisting isotropic and nematic phases of Lennard-Jones chain fluids. Solubility is described by the dimensionless Henry coefficient as defined by Equation (4).

In Figure 6, simulation results for the solubility of a Lennard-Jones gas in the coexisting isotropic and nematic phases of a linear Lennard-Jones 12-mer chain fluid are reported as a function of monomer density. A decrease in solubility with density is observed in the isotropic phase, while first an increasing and then a decreasing solubility is identified in the nematic phase. As temperature increases (see Figure 1(c)), decreasing solubilities in the isotropic phase are caused by both larger equilibrium temperatures and higher equilibrium densities, while the increasing/decreasing behaviour in the nematic phase is the consequence of a balance between larger temperatures accompanied by lower equilibrium densities. Larger solubility differences between both coexisting phases are observed at lower equilibrium temperatures.

Figure 7 shows the infinite dilution solubility of a Lennard-Jones gas in the coexisting isotropic and nematic phases of a binary mixture of linear 7- and 12-mer at constant pressure. It can be identified that the solubility difference between both phases is always larger in the mixture than in the pure components. A maximum in the isotropic-nematic solubility difference is observed at a mole fraction in the range $x_2 = 0.4 - 0.6$ from simulations and $x_2 = 0.5$ from theoretical results. This maximum is directly related to the maximum density difference shown in the previous section (see Figure 5(b)).

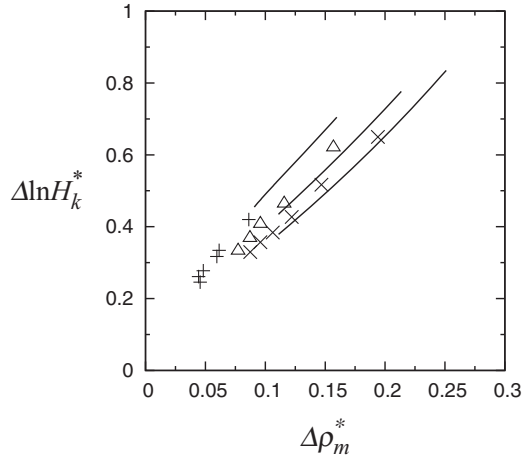

Figure 8. Solubility difference $\Delta \ln H_k^*$ as a function of reduced monomer density difference $\Delta \rho_m^*$ at the isotropic-nematic phase transition for linear Lennard-Jones 8-mer (+), 10-mer (△), and 12-mer (×) chain fluids. Solid lines are theoretical results obtained from the analytical equation of state of van Westen *et al.* [71].

Figure 8 shows the isotropic-nematic solubility difference as a function of the density difference at coexistence for the linear Lennard-Jones chain fluids. A linear

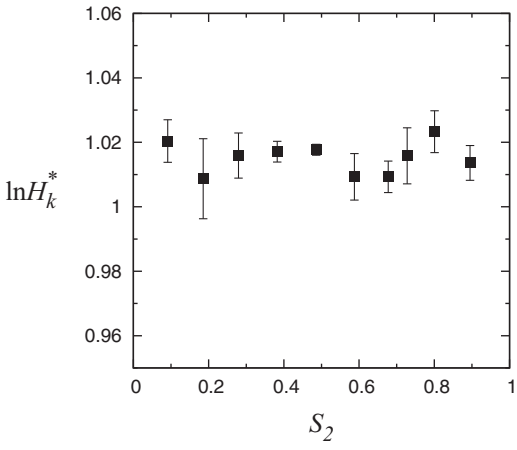

Figure 9. Infinite dilution solubility of a Lennard-Jones gas in a linear 12-mer fluid at the isotropic-nematic phase transition as a function of nematic ordering. Logarithm of dimensionless Henry coefficient ln H_k^* vs. order parameter S_2. Results are obtained at constant temperature $T^* = 10$ and monomer density $\rho_m^* = 0.42$. Error bars represent one standard deviation.

relationship between solubility difference and density difference is identified in all cases. This result indicates the central role that density has in solubility, which seems to be independent of the nematic ordering of the fluid. To confirm this supposition, we performed simulations at constant number of molecules, volume, and temperature, in the *NVT* ensemble, but restricting the nematic ordering of the system, similarly as in our previous work, Ref. [48]. Figure 9 shows the solubility of gases in a 12-mer for different values of the order parameter at constant temperature and density. From these results, it can be concluded that the solubility of a Lennard-Jones gas molecule is independent of the nematic ordering of the fluid at constant density and temperature conditions.

Figures 6 and 7 include theoretical results obtained from the equation of state of van Westen *et al.* for the same temperature range considered in the simulations (see Tables 1 and 4). These results indicate that the theory systematically underestimates the Henry coefficient. In Figure 8, we show the isotropic-nematic solubility difference as a function of density difference. It can be observed, that theory and simulations follow the same linear relationship. This underlines the fact that the differences between simulations and theory are systematic. Unfortunately, we have not found the underlying reason for these systematic differences. In Figure 8, it can be observed that density differences are overestimated by the theory, with the consequence of a higher solubility difference between the isotropic and nematic phase. The overestimation of the density difference at the isotropic-nematic transition is a common flaw of rescaled Onsager theories of the type examined in the work of van Westen *et al.*, and is expected to become less pronounced for longer chain lengths.

4. Conclusions

The isotropic-nematic phase equilibria of Lennard-Jones chain fluids were determined from direct phase equilibria calculations using an expanded version of the Gibbs ensemble.

Results for linear Lennard-Jones chain fluids showed that increasing chain length leads to a decrease of the isotropic-nematic coexistence densities and an increase of the isotropic-nematic density difference. These results are explained by a more anisotropic pair-excluded volume of longer chains, which constitutes a larger driving force for the isotropic to nematic transition. A linear relationship between coexistence pressure and temperature was found, indicating a proportional relationship between energetic and volume effects at the isotropic-nematic phase transition. We found evidence of the formation of smectic-C and crystal phases. However, these results are not conclusive due to the difficulties of the current simulation technique in representing the bulk behaviour of highly structured phases.

Simulation results were extensively compared to theoretical results as obtained from a recently developed equation of state of van Westen *et al.* [71]. It was found that the equation of state provides an excellent description of phase equilibria. The equation of state was developed based on the assumption that attractive dispersive interactions between Lennard-Jones chains do not depend on their relative orientations. The good comparison to simulation results, therefore, suggests that the effect of anisotropic dispersion interactions is small, and that a faithful description of real nematic liquid crystals could well be developed without it.

The effect of flexibility was studied by means of partially-flexible chains, consisting of a rigid linear part, and a freely-jointed part. It was found that flexibility shifts the isotropic-nematic equilibrium to larger densities and pressures. This can be explained by the fact that flexibility reduces the anisotropy of molecules, and thereby lowers the driving force for the isotropic-nematic transition.

Results for the isotropic-nematic coexistence of a binary mixture showed fractionation of the fluid into an isotropic phase richer in the short chains and a nematic phase richer in the long chains. For this mixture, a maximum in the density of the nematic phase and a maximum in the isotropic-nematic density difference at coexistence were identified. This maximum appears as a balance between a larger potential for the phase transition

as the mole fraction of the long component increases (reducing the coexisting isotropic density), and the order induced in the nematic phase by a larger presence of the long component (increasing the coexisting nematic density).

The infinite dilution solubility of a Lennard-Jones gas in Lennard-Jones chain fluids was estimated by the Widom test-particle insertion method. Results for pure components showed an increasing solubility difference between coexisting isotropic and nematic phases as temperature decreases. A linear relationship between solubility difference and density difference at coexistence was identified for all linear Lennard-Jones systems. Results for a binary mixture, at constant pressure, showed a maximum in the isotropic-nematic solubility difference as a function of mole fraction. This maximum is directly related to a maximum in the density difference between both phases. Simulations at constant temperature and density but with restricted values of the order parameter showed that the solubility of a Lennard-Jones gas is independent of the nematic ordering of the fluid.

Disclosure statement

No potential conflict of interest was reported by the authors.

Funding

This research is supported by the Stichting voor Technische Wetenschappen (Dutch Technology Foundation, STW), applied science division of the Nederlandse Organisatie voor Wetenschappelijk Onderzoek (Netherlands Organization for Scientific Research, NWO), and the Technology Program of the Ministry of Economic Affairs. In addition, this work was sponsored by the Stichting Nationale Computerfaciliteiten (National Computing Facilities Foundation, NCF) for the use of supercomputing facilities, with financial support from NWO.

References

[1] P.G. de Gennes, *The Physics of Liquid Crystals* (Oxford University Press, New York, 1974).
[2] G.R. Luckhurst and G.W. Gray, *Molecular Physics of Liquid Crystals* (Academic Press, London, 1979).
[3] L. Onsager, Ann. New York Acad. Sci. **51** (4), 627–659 (1949).
[4] M. Born, Sitz. Preuss. Akad. Wiss. **30**, 614 (1916).
[5] M. Born, Ann. Phys. **55**, 177 (1918).
[6] W. Maier and A. Saupe, Z. Nat.forsch. A **13**, 564 (1958).
[7] W. Maier and A. Saupe, Z. Nat.forsch. A **14**, 882 (1959).
[8] W. Maier and A. Saupe, Z. Nat.forsch. A **15**, 287 (1960).
[9] M.A. Cotter, J. Chem. Phys. **66** (3), 1098–1106 (1977).
[10] D. Frenkel, Physica A **263** (1–4), 26–38 (1999).
[11] M. Franco-Melgar, A.J. Haslam, and G. Jackson, Mol. Phys. **107**, 2329 (2009).
[12] S.J. Marrink, A.H. de Vries, and A.E. Mark, J. Phys. Chem. B **108** (2), 750–760 (2004).
[13] S.J. Marrink, H.J. Risselada, S. Yefimov, D.P. Tieleman, and A.H. de Vries, J. Phys. Chem. B **111** (27), 7812–7824 (2007).
[14] W.G. Noid, J. Chem. Phys. **139** (9), 090901 (2013).
[15] W.G. Noid, in *Biomolecular Simulations*, edited by L. Monticelli and E. Salonen (Humana Press, New York, 2013), Vol. 924, pp. 487–531.
[16] M.G. Saunders and G.A. Voth, Ann. Rev. Biophys. **42** (1), 73–93 (2013).
[17] S.C. Glotzer and W. Paul, Annu. Rev. Mater. Res. **32** (1), 401–436 (2002).
[18] F. Müller-Plathe, Chem. Phys. Chem. **3** (9), 754–769 (2002).
[19] B. Smit, S. Karaborni, and J.I. Siepmann, J. Chem. Phys. **102** (5), 2126–2140 (1995).
[20] C. Avendaño, T. Lafitte, C.S. Adjiman, A. Galindo, E.A. Müller, and G. Jackson, J. Phys. Chem. B **117** (9), 2717–2733 (2013).
[21] E.A. Müller and G. Jackson, Annu. Rev. Chem. Biomol. Eng. **5** (1), 405–427 (2014).
[22] T. van Westen, T.J.H. Vlugt, and J. Gross, J. Phys. Chem. B **115** (24), 7872–7880 (2011).
[23] D. Frenkel, Mol. Phys. **60** (1), 1–20 (1987).
[24] M.P. Allen, Phil. Trans. R. Soc. A **344** (1672), 323–337 (1993).
[25] C.M. Care and D.J. Cleaver, Rep. Prog. Phys. **68** (11), 2665–2700 (2005).
[26] M.R. Wilson, Chem. Soc. Rev. **36**, 1881 (2007).
[27] L. Wu, G. Jackson, and E.A. Müller, Int. J. Mol. Sci. **14** (8), 16414–16442 (2013).
[28] L. Wu, E.A. Müller, and G. Jackson, Macromolecules **47** (4), 1482–1493 (2014).
[29] W.G. Chapman, K.E. Gubbins, G. Jackson, and M. Radosz, Fluid Phase Equilib. **52** (0), 31–38 (1989).
[30] W.G. Chapman, K.E. Gubbins, G. Jackson, and M. Radosz, Ind. Eng. Chem. Res. **29** (8), 1709–1721 (1990).
[31] A. Gil-Villegas, A. Galindo, P.J. Whitehead, S.J. Mills, G. Jackson, and A.N. Burgess, J. Chem. Phys. **106** (10), 4168–4186 (1997).
[32] F.J. Blas and L.F. Vega, J. Chem. Phys. **115** (9), 4355–4358 (2001).
[33] J. Gross and G. Sadowski, Ind. Eng. Chem. Res. **40** (4), 1244–1260 (2001).
[34] E.A. Müller and K.E. Gubbins, Ind. Eng. Chem. Res. **40** (10), 2193–2211 (2001).
[35] S. Tamouza, J.P. Passarello, P. Tobaly, and J.C. de Hemptinne, Fluid Phase Equilib. **222–223** (0), 67–76 (2004).
[36] A. Lymperiadis, C.S. Adjiman, A. Galindo, and G. Jackson, J. Chem. Phys. **127** (23), 234903 (2007).
[37] C.S. Schacht, T.J.H. Vlugt, and J. Gross, J. Phys. Chem. Lett. **2** (5), 393–396 (2011).
[38] C. Avendaño, T. Lafitte, A. Galindo, C.S. Adjiman, G. Jackson, and E.A. Müller, J. Phys. Chem. B **115** (38), 11154–11169 (2011).
[39] T. Lafitte, C. Avendaño, V. Papaioannou, A. Galindo, C.S. Adjiman, G. Jackson, and E.A. Müller, Mol. Phys. **110** (11–12), 1189–1203 (2012).
[40] O. Lobanova, C. Avendaño, T. Lafitte, E.A. Müller, and G. Jackson, Mol. Phys. **113** (9–10), 1228–1249 (2015).

[41] A. Hemmen, A.Z. Panagiotopoulos, and J. Gross, J. Phys. Chem. B **119** (23), 7087–7099 (2015).
[42] A. Hemmen and J. Gross, J. Phys. Chem. B **119** (35), 11695–11707 (2015).
[43] M. Whittle and A. Masters, Mol. Phys. **72** (2), 247–265 (1991).
[44] M.R. Wilson and M.P. Allen, Mol. Phys. **80** (2), 277–295 (1993).
[45] D.C. Williamson and G. Jackson, J. Chem. Phys. **108** (24), 10294–10302 (1998).
[46] A. Yethiraj and H. Fynewever, Mol. Phys. **93** (5), 693–701 (1998).
[47] C. Vega, C. McBride, and L.G. MacDowell, J. Chem. Phys. **115** (9), 4203–4211 (2001).
[48] B. Oyarzún, T. van Westen, and T.J.H. Vlugt, J. Chem. Phys. **138** (20), 204905 (2013).
[49] B. Oyarzún, T. van Westen, and T.J.H. Vlugt, J. Chem. Phys. **142** (6), 064903 (2015).
[50] D. Frenkel, B.M. Mulder, and J.P. McTague, Phys. Rev. Lett. **52**, 287 (1984).
[51] M.P. Allen, Liq. Cryst. **8** (4), 499–511 (1990).
[52] A. Samborski, G.T. Evans, C.P. Mason, and M.P. Allen, Mol. Phys. **81** (2), 263–276 (1994).
[53] A. Stroobants, H.N.W. Lekkerkerker, and D. Frenkel, Phys. Rev. A **36**, 2929 (1987).
[54] J.A.C. Veerman and D. Frenkel, Phys. Rev. A **41**, 3237 (1990).
[55] P. Bolhuis and D. Frenkel, J. Chem. Phys. **106** (2), 666–687 (1997).
[56] B.J. Berne and P. Pechukas, J. Chem. Phys. **56** (8), 4213–4216 (1972).
[57] J.G. Gay and B.J. Berne, J. Chem. Phys. **74** (6), 3316–3319 (1981).
[58] D. Adams, G. Luckhurst, and R. Phippen, Mol. Phys. **61** (6), 1575–1580 (1987).
[59] E. de Miguel, L.F. Rull, M.K. Chalam, and K.E. Gubbins, Mol. Phys. **74** (2), 405–424 (1991).
[60] M. Bates and G. Luckhurst, in *Liquid Crystals I*, edited by D. Mingos and P. Michael (Springer, Berlin, 1999), Vol. 94, pp. 65–137.
[61] C. Zannoni, J. Mater. Chem. **11**, 2637 (2001).
[62] D.C. Williamson and F. del Rio, J. Chem. Phys. **109** (11), 4675–4686 (1998).
[63] B. Martínez-Haya, L.F. Rull, A. Cuetos, and S. Lago, Mol. Phys. **99** (6), 509–516 (2001).
[64] A. Cuetos, B. Martínez-Haya, L.F. Rull, and S. Lago, J. Chem. Phys. **117** (6), 2934–2946 (2002).
[65] A. Cuetos, B. Martínez-Haya, S. Lago, and L.F. Rull, Phys. Rev. E **68**, 011704 (2003).
[66] J.S. Lintuvuori and M.R. Wilson, J. Chem. Phys. **128** (4), 044906 (2008).
[67] A. Cuetos and B. Martínez-Haya, Mol. Phys. **113** (9–10), 1137–1144 (2015).
[68] M.R. Wilson, J. Chem. Phys. **107** (20), 8654–8663 (1997).
[69] Z.E. Hughes, L.M. Stimson, H. Slim, J.S. Lintuvuori, J.M. Ilnytskyi, and M.R. Wilson, Comput. Phys. Commun. **178** (10), 724–731 (2008).
[70] J.S. Lintuvuori and M.R. Wilson, Phys. Chem. Chem. Phys. **11**, 2116 (2009).
[71] T. van Westen, B. Oyarzún, T.J.H. Vlugt, and J. Gross, J. Chem. Phys. **142** (24), 244903 (2015).
[72] A. Galindo, C. Vega, E. Sanz, L.G. MacDowell, E. de Miguel, and F.J. Blas, J. Chem. Phys. **120** (8), 3957–3968 (2004).
[73] J. Gross and P.J. Jansens, WO2008147181-A1/NL2000654-C2 (Dec. 4, 2008).
[74] M. de Groen, T.J.H. Vlugt and T.W. de Loos, J. Phys. Chem. B **116** (30), 9101–9106 (2012).
[75] M. de Groen, H. Matsuda, T.J.H. Vlugt, and T.W. de Loos, J. Chem. Thermodyn. **59** (0), 20–27 (2013).
[76] M. de Groen, B.C. Ramaker, T.J.H. Vlugt, and T.W. de Loos, J. Chem. Eng. Data **59** (5), 1667–1672 (2014).
[77] M. de Groen, T.J.H. Vlugt, and T.W. de Loos, AIChE J, **61** (9), 2977–2984 (2015).
[78] D.S. Chen, G.H. Hsiue, J.D. Schultze, B. Song, and J. Springer, Mol. Cryst. Liq. Cryst. **237** (1), 85–95 (1993).
[79] G.H. Chen and J. Springer, Mol. Cryst. Liq. Cryst. **339**(1), 31–44 (2000).
[80] W.E. Acree and J.S. Chickos, J. Phys. Chem. Ref. Data **35**(3), 1051–1330 (2006).
[81] T. van Westen, T.J.H. Vlugt, and J. Gross, J. Chem. Phys. **137** (4), 044906 (2012).
[82] F.A. Escobedo and J.J. de Pablo, J. Chem. Phys. **105** (10), 4391–4394 (1996).
[83] W. Shi and E.J. Maginn, J. Comput. Chem. **29** (15), 2520–2530 (2008).
[84] F.A. Escobedo and J.J. de Pablo, J. Chem. Phys. **103** (7), 2703–2710 (1995).
[85] F.A. Escobedo, J. Chem. Phys. **127** (17), 174104 (2007).
[86] W. Shi and E.J. Maginn, J. Chem. Theory Comput. **3** (4), 1451–1463 (2007).
[87] A. Torres-Knoop, S.P. Balaji, T.J.H. Vlugt, and D. Dubbeldam, J. Chem. Theory Comput. **10** (3), 942–952 (2014).
[88] F. Wang and D.P. Landau, Phys. Rev. Lett. **86**, 2050 (2001).
[89] F. Wang and D.P. Landau, Phys. Rev. E **64**, 056101 (2001).
[90] M.P. Allen and D.J. Tildesley, *Computer Simulation of Liquids* (Oxford University Press, Oxford, 1989).
[91] D. Frenkel and B. Smit, *Understanding Molecular Simulations*, 2nd ed. (Academic Press, London, 2002).
[92] D.N. Theodorou, T.D. Boone, L.R. Dodd, and K.F. Mansfield, Macromol. Theory Simul. **2** (2), 191–238 (1993).
[93] C.M. Wijmans, B. Smit, and R.D. Groot, J. Chem. Phys. **114** (17), 7644–7654 (2001).
[94] R. Eppenga and D. Frenkel, Mol. Phys. **52** (6), 1303–1334 (1984).
[95] R.B. Meyer and T.C. Lubensky, Phys. Rev. A **14**, 2307 (1976).
[96] J.M. Polson and D. Frenkel, Phys. Rev. E **56**, R6260 (1997).
[97] K.S. Shing and K.E. Gubbins, Mol. Phys. **46** (5), 1109–1128 (1982).
[98] B. Widom, J. Chem. Phys. **39** (11), 2808–2812 (1963).
[99] J.K. Shah and E.J. Maginn, J. Phys. Chem. B **109** (20), 10395–10405 (2005).
[100] J.A. Barker and D. Henderson, J. Chem. Phys. **47** (8), 2856–2861 (1967).
[101] J.A. Barker and D. Henderson, J. Chem. Phys. **47** (11), 4714–4721 (1967).

[102] T. van Westen, B. Oyarzún, T.J.H. Vlugt, and J. Gross, Mol. Phys. **112** (7), 919–928 (2014).
[103] T. van Westen, B. Oyarzún, T.J.H. Vlugt, and J. Gross, J. Chem. Phys. **139** (3), 034505 (2013).
[104] T. van Westen, T.J.H. Vlugt, and J. Gross, J. Chem. Phys. **140** (3), 034504 (2014).
[105] T. van Westen, T.J.H. Vlugt, and J. Gross, J. Chem. Phys. **142** (22), 224504 (2015).
[106] D.C. Williamson and G. Jackson, Mol. Phys. **86** (4), 819–836 (1995).
[107] F. Affouard, M. Kröger, and S. Hess, Phys. Rev. E **54**, 5178 (1996).
[108] C. Vega, E.P.A. Paras, and P.A. Monson, J. Chem. Phys. **96**, 9060 (1992).
[109] J.M. Polson and D. Frenkel, J. Chem. Phys. **109** (1), 318–328 (1998).
[110] R. Agrawal and D.A. Kofke, Mol. Phys. **85** (1), 23–42 (1995).
[111] M.B. Sweatman, Mol. Simul. **35**(10–11), 897–909 (2009).
[112] E. de Miguel and C. Vega, J. Chem. Phys. **117** (13), 6313–6322 (2002).
[113] P. Mishra and J. Ram, Eur. Phys. J. E **17** (3), 345–351 (2005).
[114] B. Martínez-Haya and A. Cuetos, J. Phys. Chem. B **111** (28), 8150–8157 (2007).